DAC REPORT 59518

# DUCTILITY LIMITATIONS OF ALUMINUM-SILICON ALLOYS

GPO PRICE        $ _____

CFSTI PRICE(S) $ _____

Hard copy (HC) ___*9. 00*___

Microfiche (MF) ___*150*___

ff 653 July 65

N 66.   3. 8. 7. 9. 1

# MISSILE & SPACE SYSTEMS DIVISION
## DOUGLAS AIRCRAFT COMPANY, INC.
### SANTA MONICA CALIFORNIA

*DOUGLAS*

DAC REPORT 59518

# DUCTILITY LIMITATIONS OF ALUMINUM-SILICON ALLOYS

Prepared by:
S. Frederick
and
W. A. Bailey

METALS-CERAMICS BRANCH

8-19-66

*DOUGLAS*

Prepared for National Aeronautics
and Space Administration
Marshall Space Flight Center
Huntsville, Alabama, Contract NASA 7-101

Approved by G. V. Bennett, Branch Chief
Metals-Ceramics
Materials Research & Production
Methods Department

CATALOG NO. PDL 70262

27

## ABSTRACT

The relation between microstructure and mechanical properties of cast 356 type aluminum alloys was studied to determine the cause of the variations in properties resulting from differences in solidification rate. It was found that variations in strength are a consequence of variations in ductility and that ductility is inversely proportional to the dendrite cell size. A mechanism is proposed to account for this correlation based on the fracture strain of the interdendritic silicon particles, and the differential strain across dendrite cell boundaries.

## 1. INTRODUCTION

An empiricism of long standing is that permanent-mold castings of aluminum have better properties than sand castings. The reasons usually given are finer grain structure and reduction in porosity (Reference 1). In studies of fatigue strength variations with solidification rate of A356-T6, Bailey (References 2 and 3) found a systematic variation of static properties as well. Of particular interest is the observation that for a given composition and heat treatment, the ductility as well as the ultimate strength increased with increased solidification rate. Since the composition and microstructure of this alloy system are similar to those found in aluminum welds, a study was initiated to determine the details of how higher cooling rates improve the mechanical properties of Al-Si alloys. The results of this study are presented here.

## 2. EXPERIMENTAL PROCEDURE

While much of the previously obtained data were available, the specimens were not. Because electron fractographs were desired as well as transmission electron micrographs, a series of specimens was prepared using 356-T6 rather than the A356-T6 alloy used in the earlier studies. This allowed a comparison of behaviors of alloys with substantially different strengths but with only small differences in alloy composition. The composition and heat treatment of both alloys are given in Table I. The specimens were cut from a cast MIT chill plate (Reference 4) in the same manner as previous studies. A photograph of the original casting is shown in Figure 1. Since one end is heavily chilled, and the other end has a large riser, solidification is essentially unidirectional from the chill end to the riser. Cooling through the solidification range takes

1

## TABLE I — COMPOSITIONS AND HEAT TREATMENTS

Composition

| Element | A356 | 356 |
|---------|------|-----|
| Si | 6.9 | 6.7 |
| Mg | 0.47 | 0.28 |
| Be | 0.05 | Nil |
| Fe | 0.13 | 0.11 |
| Ti | 0.20 | 0.06 |
| Cu | Nil | 0.02 |
| Zn | Nil | Nil |
| Mn | Nil | Nil |
| Cr | Nil | Nil |
| Al | Bal | Bal |

Heat Treatment

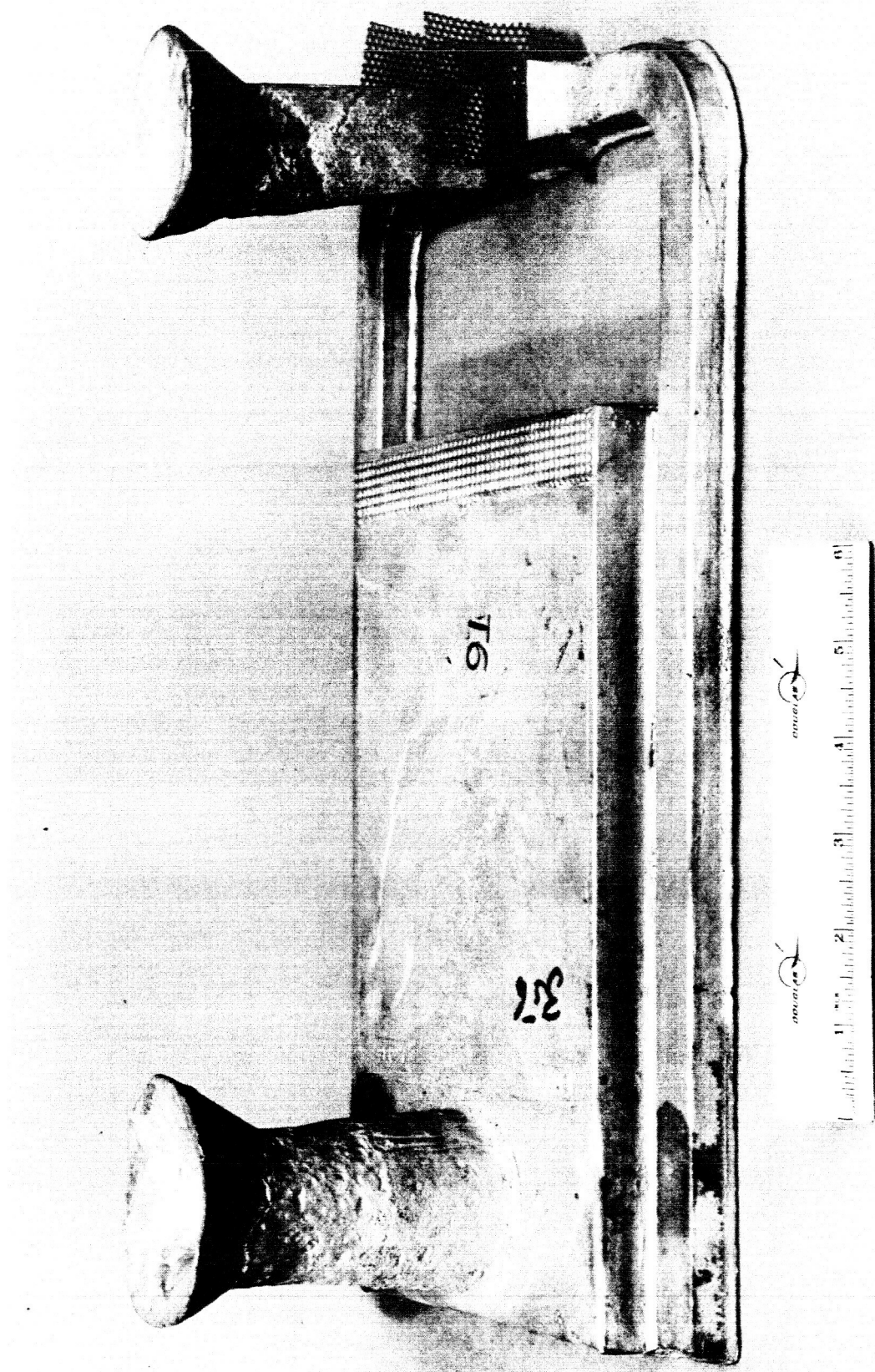| | A356-T6 | | 356-T6 |
|---|---|---|---|
| | Series 1 | Series 2 | |
| Solution H.T. | | | |
| Temp. | 1010°F (543°C) | | 1010°F (543°C) |
| Time | 10 hr. | | 10 hr. |
| Quench | 140°F (60°C) Water | | 80°F (26°C) water |
| Aging | | | |
| Temp. | 320°F (160°C) | 350°F (177°C) | 320°F (160°C) |
| Time | 7.25 hr. | 7.25 hr. | 3 hr. |

FIGURE 1 – MIT CHILL PLATE

a few seconds at the chill end but may take five minutes near the riser

(Reference 2). By cutting slabs from the plate, parallel to the chill,

a group of specimens is obtained which represents different cooling rates,

but have essentially the same composition. For the present tests, 0.125

and 0.250-in thick slabs were cut and machined to the configuration

shown in Figure 2. The thicker specimens were tested to failure at 2000

lb/min while the thinner specimens were tested in an Instron machine at a

constant cross-head speed of 0.02 in/min. These thin specimens were

intended for transmission electron microscopy. Therefore, some of them

were tested to failure while the remainder were given various amounts of

pre-strain.

Dendrite cell sizes were measured by the linear intercept method on

photomicrographs at either 100 X or 50 X, depending on the cell size.

Determinations were made on two mutually perpendicular planes and an

RMS average taken.

Electron fractographs of representative tensile specimens were made in

the conventional manner using the two-stage replica technique

(Reference 5).

To prepare samples for transmission electron microscopy, pre-strained

(or fractured) tensile specimens were chemically milled as thin as

possible while still maintaining a reasonable flatness. The solution

used was a sulfone-buffered sodium hydroxide solution at about 85°C

(185°F). The next step was to electropolish in a solution of 50 cc

$HNO_3$, 50 cc $H_2O$, 2cc HCl, to the point of perforations. It was found

that intermittent chemical polishing in CP4A (5cc $HNO_3$, 3ccHAc, 3cc HF)

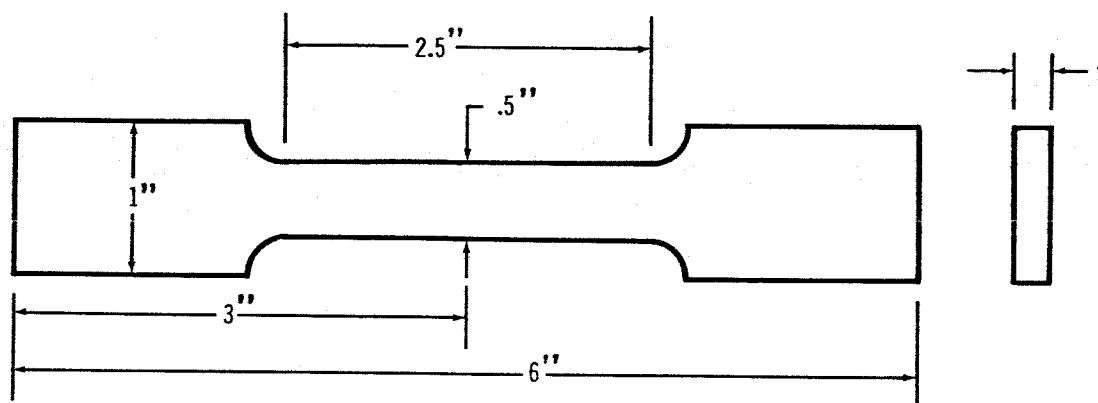was helpful during this step. Final polishing was by the method of

Figure 2. Tensile Specimen

Despres (Reference 6), in which small pieces of pre-thinned samples were welded between two stainless steel washers, and the composite electropolished. The electrolyte used in this step was 817cc $H_3PO_4$, 34cc $H_2SO_4$, 156g Chromic acid, and 40cc $H_2O$, used at 65°C (149°F). Intermittent dipping in CP4A was helpful here too.

3.  ## RESULTS AND DISCUSSION

The results of the tensile tests and the dendrite cell size determinations are given in Table 2 and Figures 3 and 4. Included in Figures 3 and 4 are Bailey's previous results (References 2 and 3). The present data for 356-T6 and the previous data for A356-T6 all show the same trends, namely, a decrease in ultimate strength and elongation with increasing solidification time and a corresponding increase in dendrite cell size. The yield strength is essentially constant. (It should be noted that if measurements are made very close to the riser, a drop in yield strength is noted as a consequence of casting defects. Consideration of such defects was not part of the present program and all results reported here are for radiographically sound material.) This constancy of the yield strength is particularly significant since it indicates these variations in solidification rate do not affect the stress required to initiate plastic flow. By plotting true stress-true strain curves as in Figure 5, it can be seen that not only is the yield strength constant but so is the rate of work hardening. It would appear that the effect of solidification time is to limit in some way, the maximum amount of strain. This in turn, gives rise to a variation in ultimate strength. It might be argued that the prime consideration is actually the ultimate strength which then controls the strain. It is difficult to see, however, how such a mechanism could apply to the alloys

## TABLE 2 - DENDRITE CELL SIZES AND TENSILE TEST RESULTS

| Distance From Chill (in) | Mean Dendrite Cell Diameter (in X $10^3$) | $F_{ty}$ (KSI) | $F_{tu}$ (KSI) | Elongation in 2 in. (%) |
|---|---|---|---|---|
| **A356-T6 Series 1** | | | | |
| 0.5 | 1.41 | 36.7 | 50.6 | 13.5 |
|  |  | 35.2 | 49.7 | 15.0 |
| 1.0 | 1.54* | 37.3 | 50.4 | 12.5 |
|  |  | 35.8 | 48.8 | 11.0 |
| 1.5 | 1.67* | 36.0 | 48.8 | 11.0 |
|  |  | 36.1 | 49.5 | 10.0 |
| 2.0 | 1.87 | 36.6 | 49.3 | 10.0 |
| 2.5 | 2.00 | 34.1 | 47.9 | 9.0 |
| 3.5 | 2.12 | 34.7 | 47.1 | 8.0 |
| 4.0 | 2.30* | 35.9 | 47.0 | 6.0 |
| 5.5 | 2.68* | 34.2 | 44.6 | 4.5 |
| 6.0 | 2.83 | 35.5 | 45.5 | 4.0 |
| 7.5 | 3.20* | 34.2 | 42.2 | 2.5 |
| 8.0 | 3.46 | 35.0 | 43.3 | 3.5 |
| **A356-T6 Series 2** | | | | |
| 0.5 | 1.41 | 42.7 | 50.3 | 11.0 |
|  |  | 41.9 | 50.3 | 10.0 |
| 1.5 | 1.67* | 42.9 | 49.6 | 11.0 |
|  |  | 40.9 | 49.3 | 10.0 |
| 2.5 | 2.00 | 42.4 | 49.4 | 8.0 |
|  |  | 42.1 | 49.0 | 8.0 |
| 3.5 | 2.12 | 43.4 | 48.9 | 5.0 |
|  |  | 42.2 | 48.4 | 5.0 |
| 4.5 | 2.35 | 42.2 | 48.3 | 4.0 |
|  |  | 42.1 | 48.0 | 4.5 |
| 5.5 | 2.68* | 42.1 | 47.9 | 3.0 |
|  |  | 42.3 | 47.4 | 3.0 |
| 6.5 | 2.92 | 42.3 | 47.2 | 2.0 |
|  |  | 42.2 | 46.4 | 2.0 |
| 7.5 | 3.20* | 42.1 | 45.6 | 1.0 |
|  |  | 42.0 | 46.0 | 1.5 |

* Interpolated Values from Figure 4.

TABLE 2 (Cont'd.)

| Distance From Chill (in) | Mean Dendrite Cell Diameter (in X $10^3$) | $F_{ty}$ (KSI) | $F_{tu}$ (KSI) | Elongation in 2 in. (%) |
|---|---|---|---|---|
| 356-T6 | | | | |
| 0.19 | 1.41* | 30.7 | 41.7 | 9.0 |
| 0.50 | 1.62 | 30.7 | 41.2 | 6.0 |
| 1.38 | 2.30 | 30.1 | 39.9 | 5.5 |
| 1.94 | 2.60* | 30.8 | 38.7 | 3.5 |
| 2.25 | 2.89 | 30.4 | 39.1 | 3.0 |
| 3.12 | 3.42 | 31.2 | 38.2 | 2.0 |
| 3.44 | 3.65* | 31.6 | 37.5 | 2.5 |
| 4.00 | 4.04 | 30.1 | 36.7 | 1.5 |
| 4.88 | 4.09 | 31.8 | 35.7 | 1.0 |
| 5.19 | 4.20* | 30.9 | 34.5 | 1.0 |
| 5.75 | 4.44 | 31.0 | 34.0 | 1.0 |
| 6.62 | 4.81 | 30.7 | 31.4 | 1.0 |
| 6.93 | 4.86* | ---** | 28.6 | 1.0 |
| 7.50 | 4.98 | 29.8 | 30.4 | 1.0 |

 * Interpolated values from Figure 4
** Did not reach 0.2% offset strain
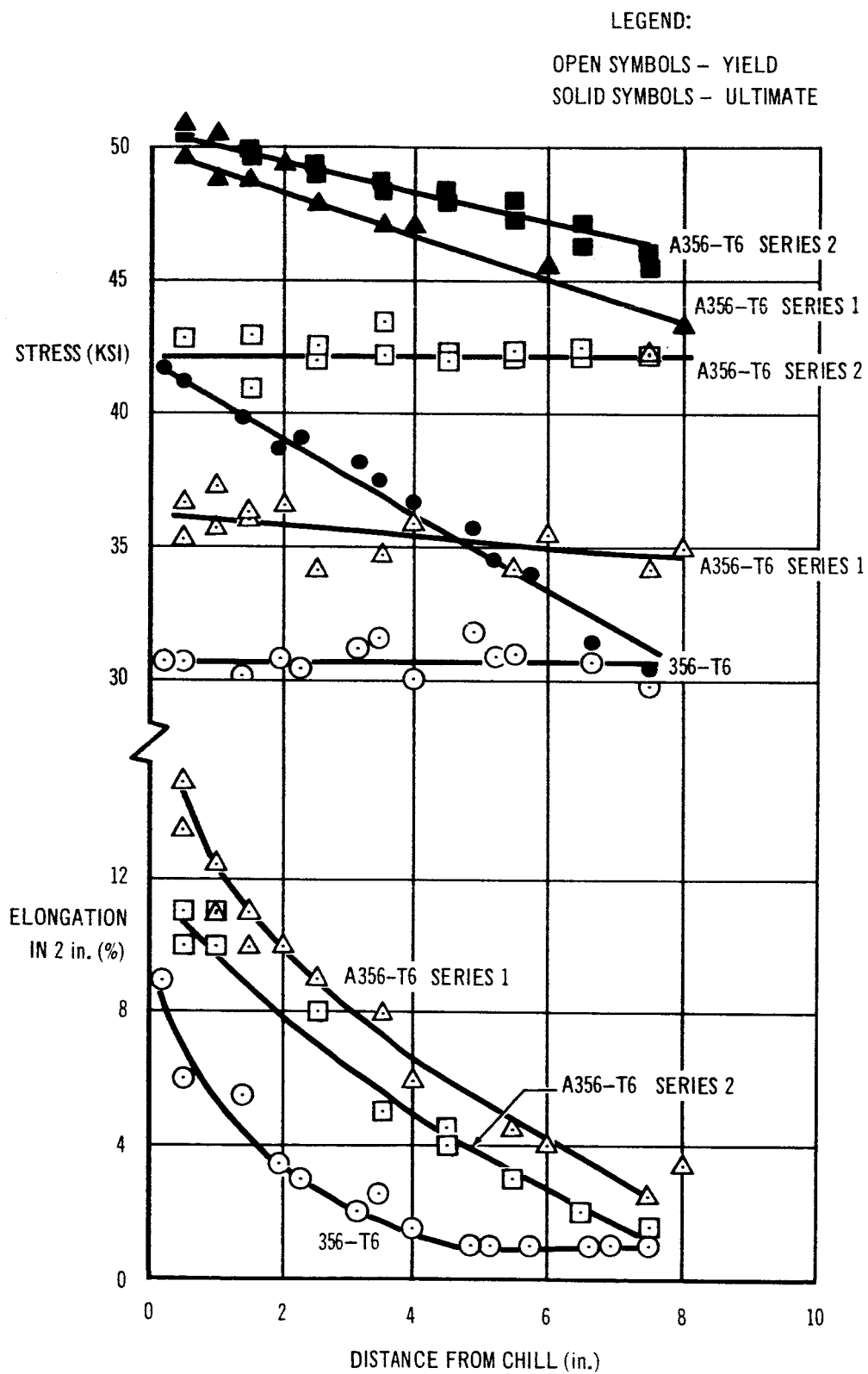
Figure 3. Tensile Test Results
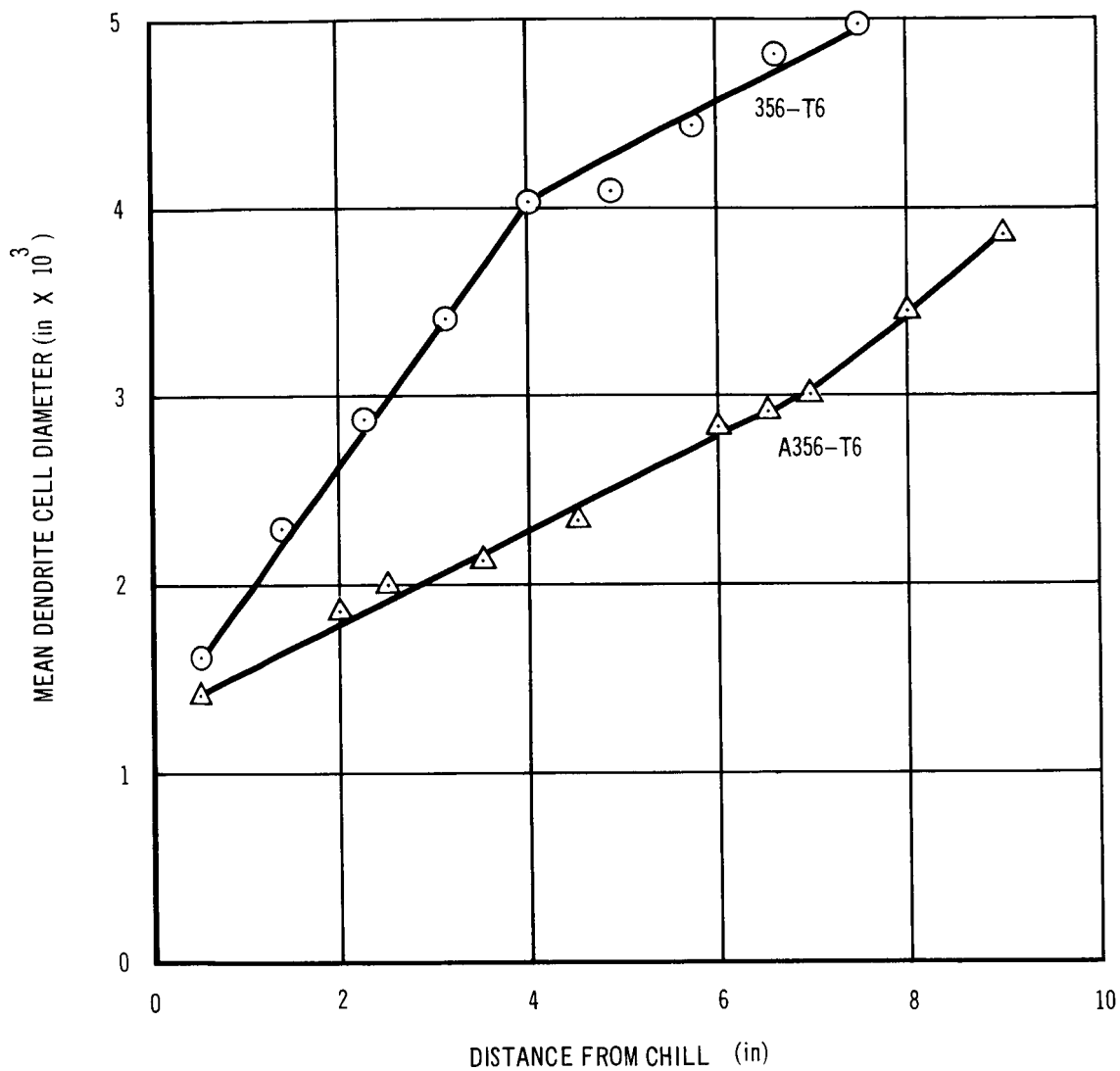
Figure 4. Mean Dendrite Cell Size
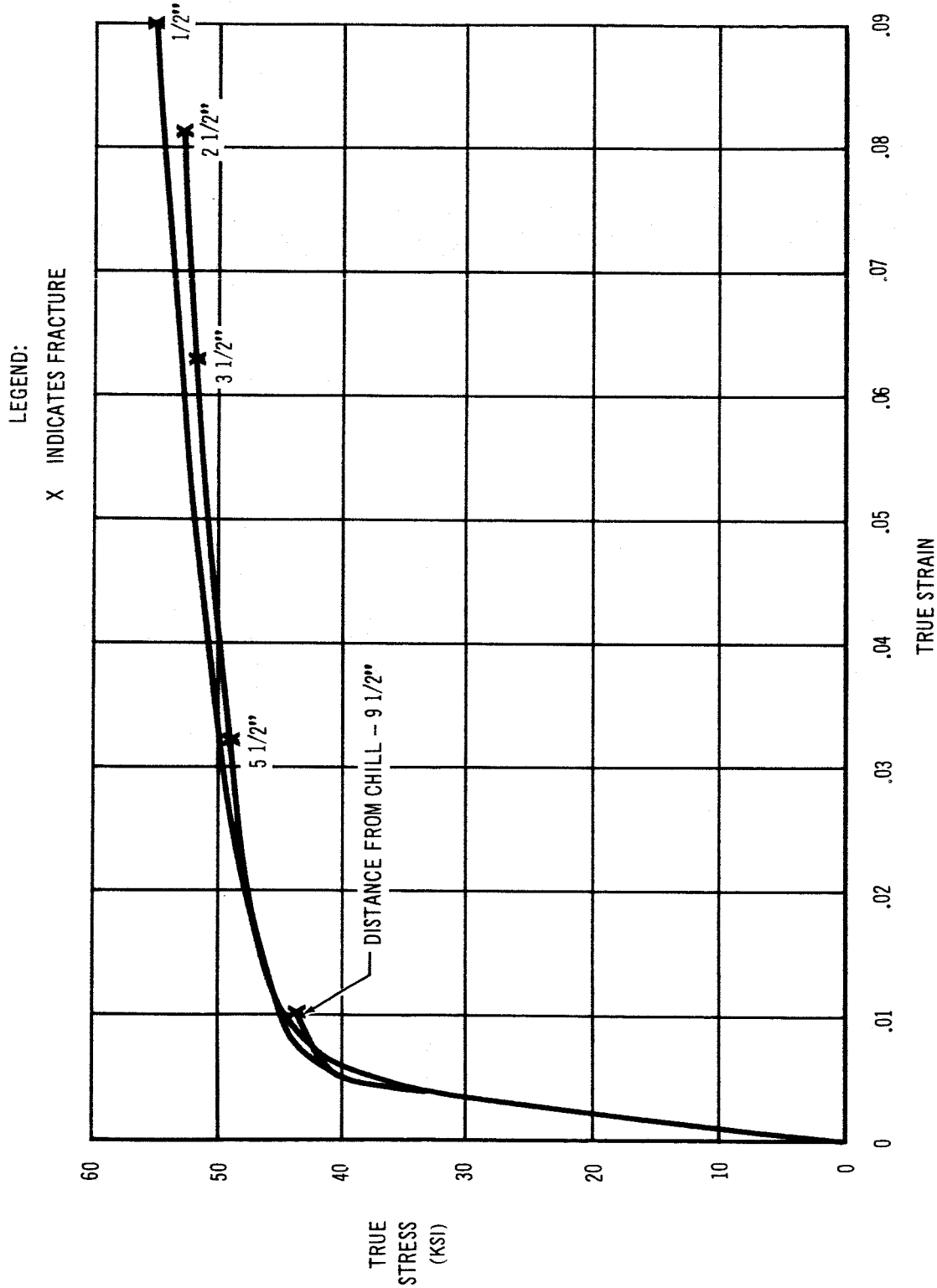
Figure 5. True Stress – True Strain Curves A356 –T6 (Series 2) Aging Temperature 350° F

considered here, with such large variations in yield and ultimate strengths, but with such similar microstructures and compositions.

The microstructures of both 356-T6 and A356-T6 (Figures 6 and 7) consist of primary silicon particles outlining dendrite cells. This structure is not altered by the normal heat treatments given these alloys. Fracture paths, as seen in Figure 8, are almost exclusively through the dendrite cell boundaries. Furthermore, the silicon particles along the fracture path are usually broken rather than pulled out of the matrix. In fact, near the fracture surface, it is often possible to find broken silicon particles whose direction of fracture is usually normal to the tensile axis, even if this is the longest path in the particle. Examples are shown in Figure 9. Electron fractographs such as those in Figures 10 and 11 show that the silicon particles exhibit brittle fracture, which is expected. These fractographs also show that the region immediately adjacent to the silicon particles were typically stretched areas. This type of surface is indicative of substantial plastic flow (Reference 5). Insofar as fractographic behavior is concerned, there was no difference between specimens slowly cooled and those near the chill. These observations indicate initial fracture of the silicon particles which may extend into the aluminum matrix. These initial fractures then propagate in a ductile manner.

The distribution of dislocations, as observed by transmission electron microscopy, appears to be quite uniform. Typical examples are given in Figures 12 - 18. There are many loops and jogs indicating extensive cross-slip. Very few heavy tangles were noted and no real sign of cell formation. The dislocation density increased with strain. Although it was quite difficult to thin areas around the silicon particles and
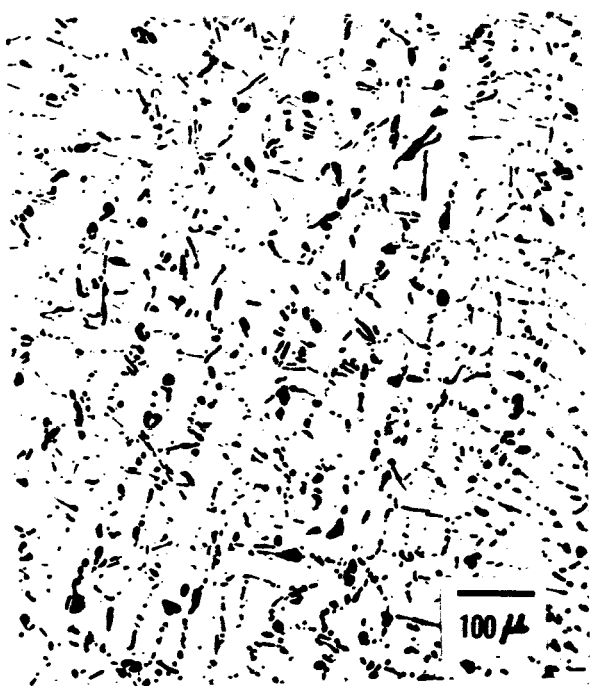
0.5 in. From Chill
M23374
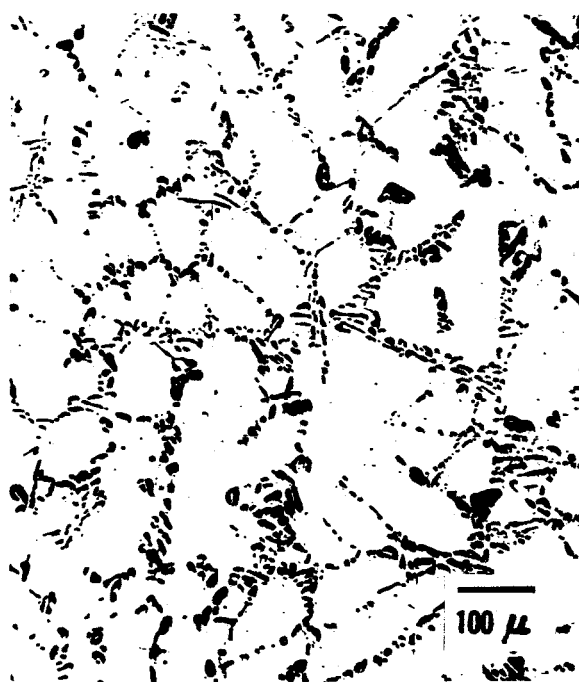
2.25 in. From Chill
M23376

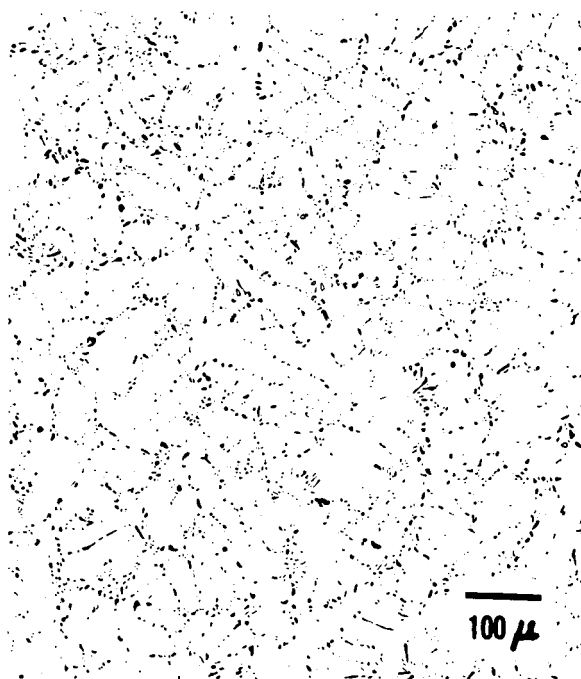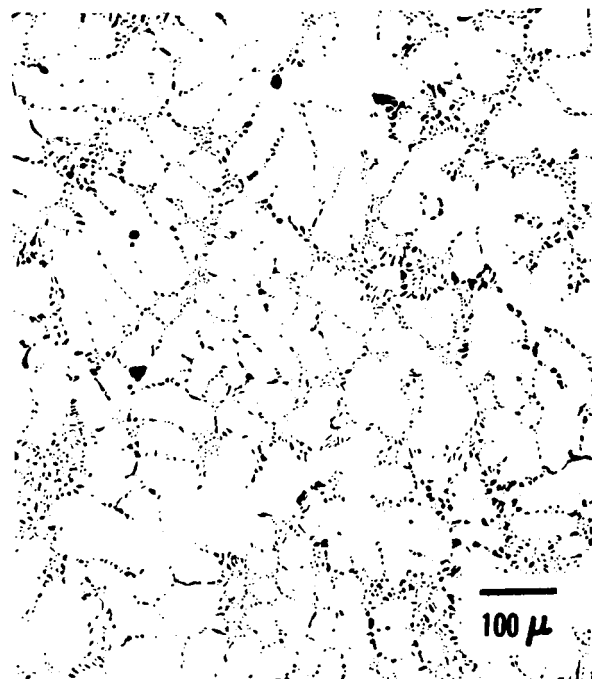4.88 in. From Chill
M 23378

7.5 in. From Chill
M23382

FIGURE 6 - MICROSTRUCTURES OF 356-T6 SPECIMENS

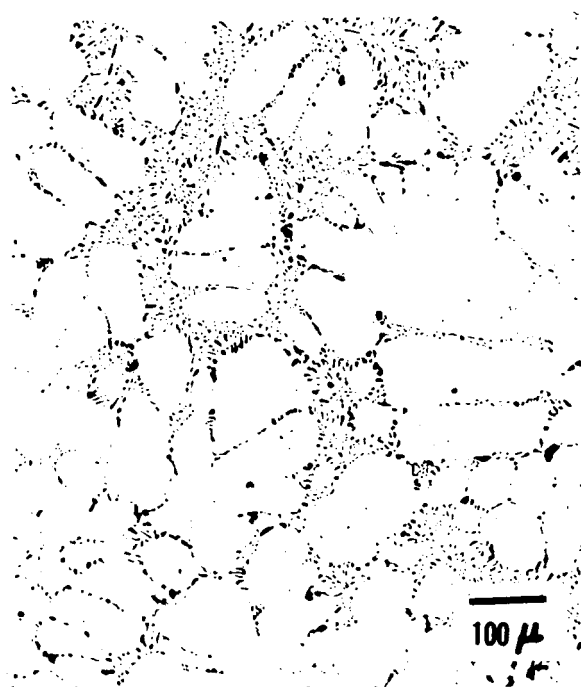Plane of Polish is Normal to Direction of
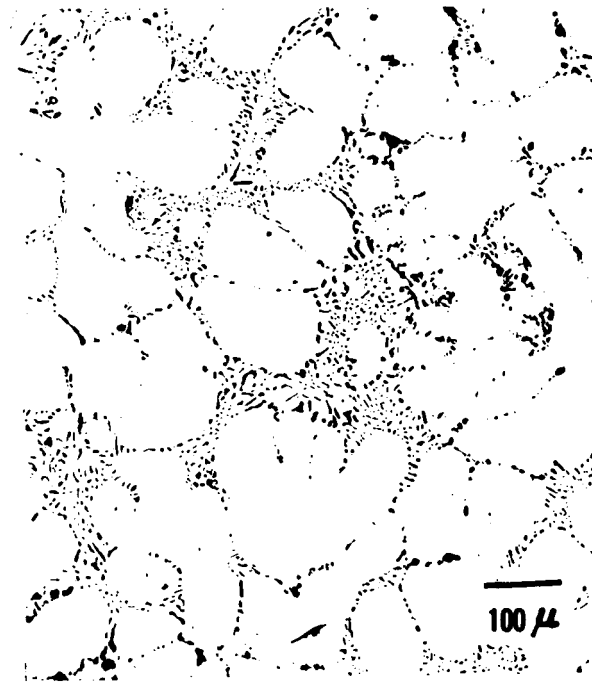Solidification.

Unetched.   Original Magnification 100X

13

0.5 In. From Chill
M17301

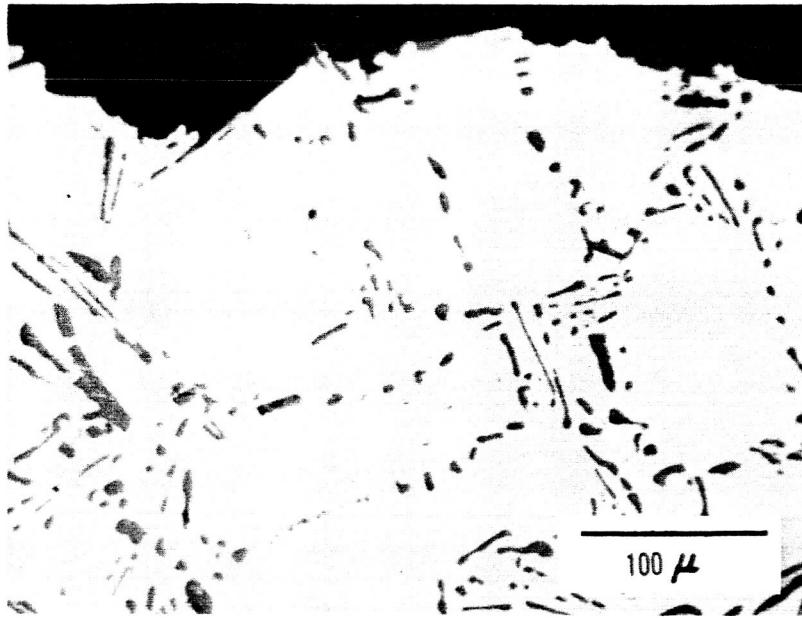1.5 In. From Chill
M17302

3.5 In. From Chill
M17303

6.0 In. From Chill
M17304

FIGURE 7 - MICROSTRUCTURES OF A356-T6 SPECIMENS

Plane of Polish is Normal to Direction of
Solidification
Unetched.  Original Magnification 100X
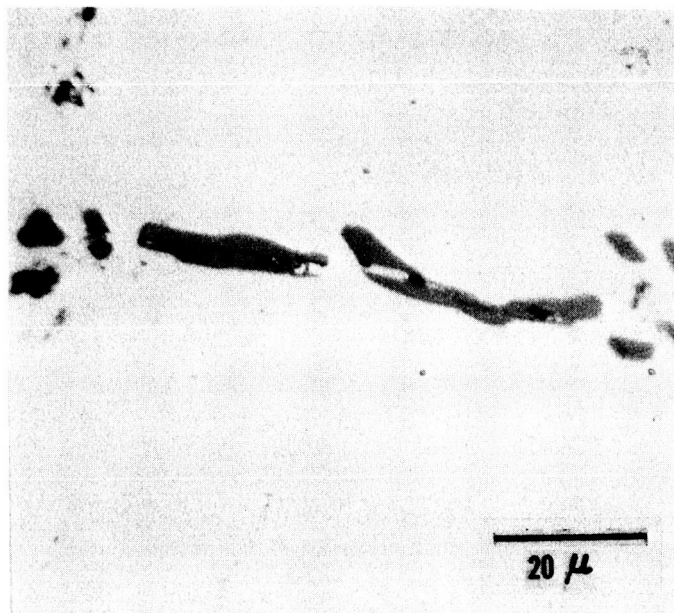
14

3.12-In. From Chill                M24205



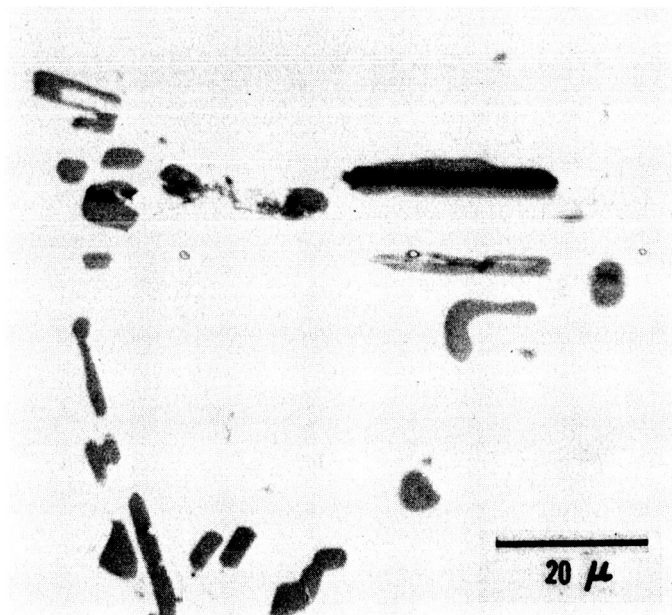6.62-In. From Chill                M24204

FIGURE 8 - FRACTURE PATHS IN 356-T6

Unetched.   Original Magnification 250X

3.12-In. From Chill          M24203



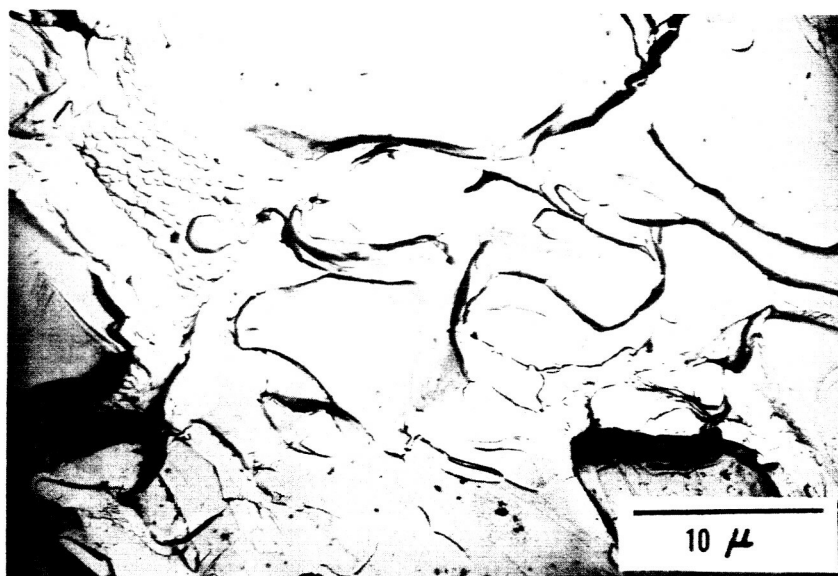4.0-In. From Chill          M24202

FIGURE 9 - TYPICAL PARTICLE FRACTURES NEAR FRACTURE
SURFACE OF 356-T6

Unetched.  Original Magnification 1000X

0.5-In. From Chill　　　　　E13038



1.38-In. From Chill　　　　　E13043

FIGURE 10 - ELECTRON FRACTOGRAPHS OF 356-T6

Two-Stage Plastic Carbon Replica
Chromium Shadowed at 45°

4.0-In. From Chill                                           E12996



5.75-In. From Chill                                          E13044
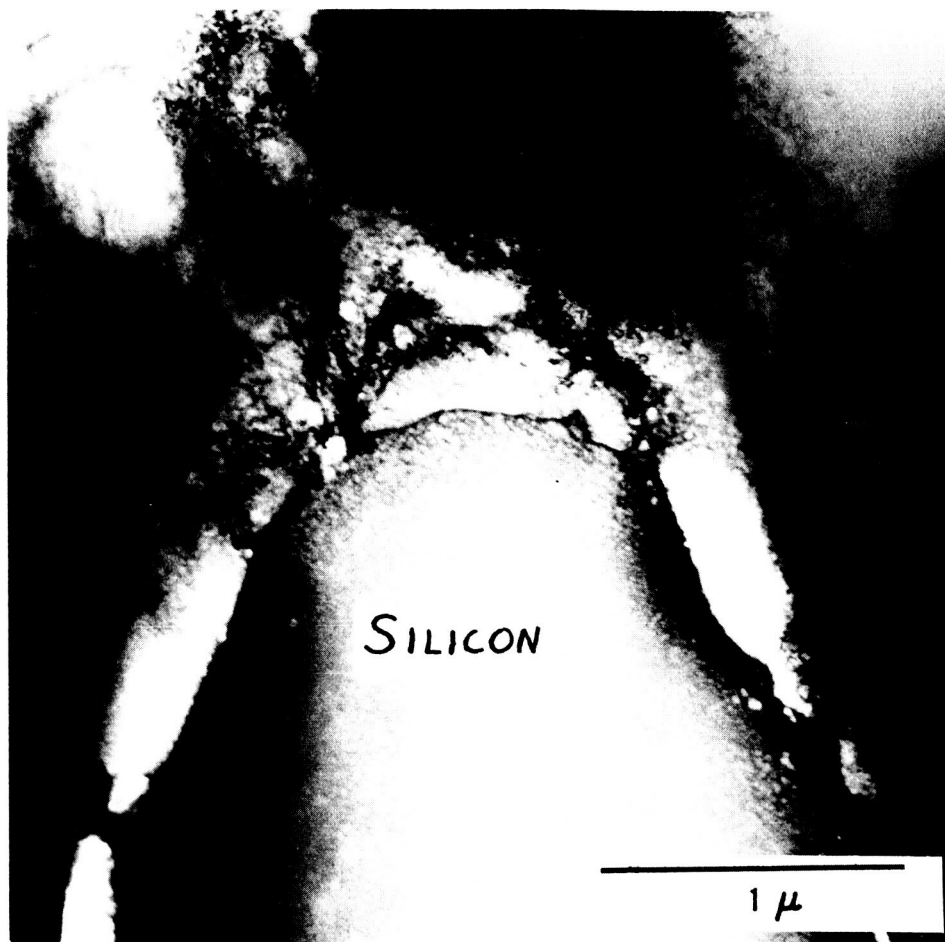
FIGURE 11 - ELECTRON FRACTOGRAPHS OF 356-T6

Two-Stage Plastic Carbon Replica
Chromium Shadowed at 45°

18

1 μ

E13111

FIGURE 12 - TRANSMISSION ELECTRON MICROGRAPH OF 356-T6

Distance From Chill 0.19 In.
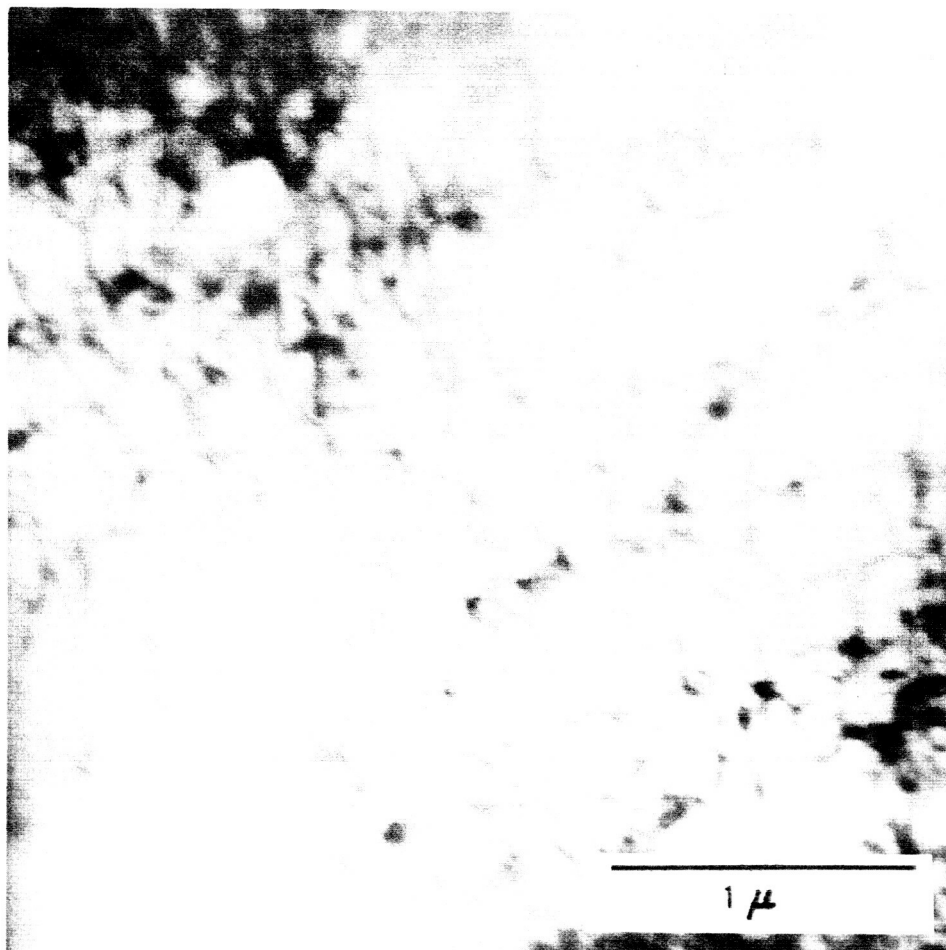Strain 9% Elongation (Fractured Specimen)

SILICON

1 μ

E13109

FIGURE 13 - ELECTRON TRANSMISSION MICROGRAPH OF 356-T6
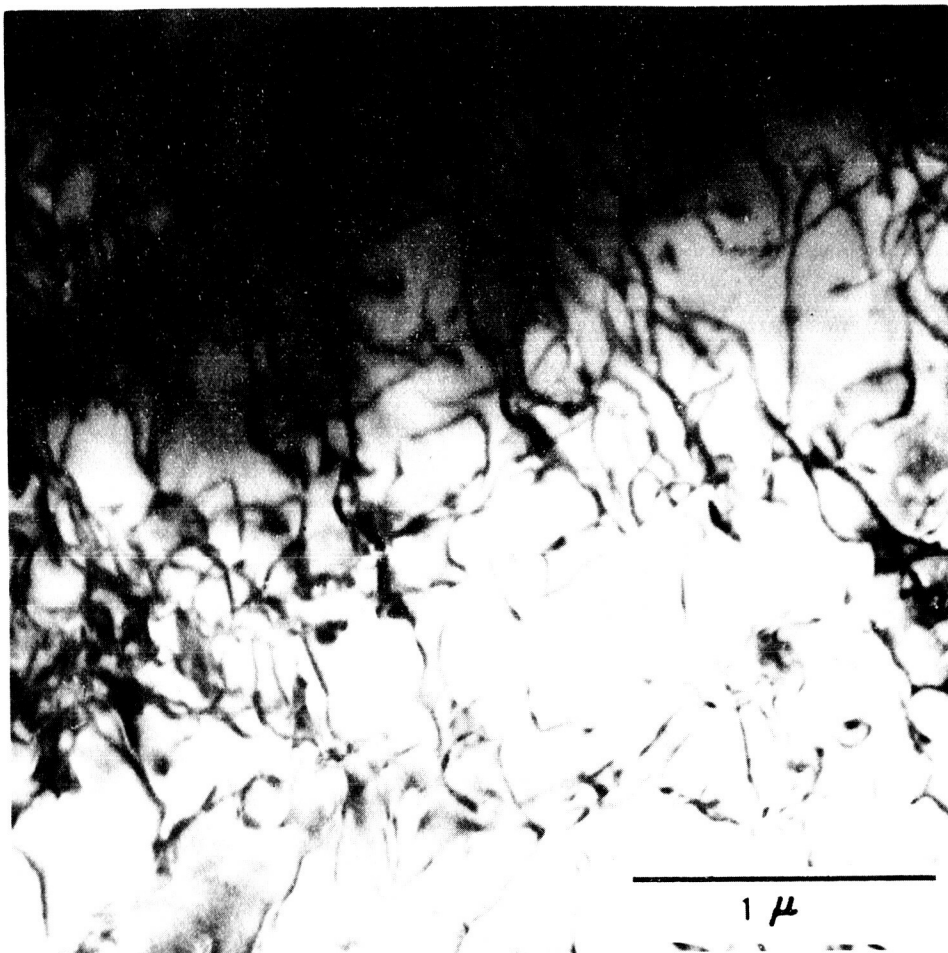
Distance From Chill - 0.19 In.
Strain - 9% Elongation (Fractured Specimen)

E13091
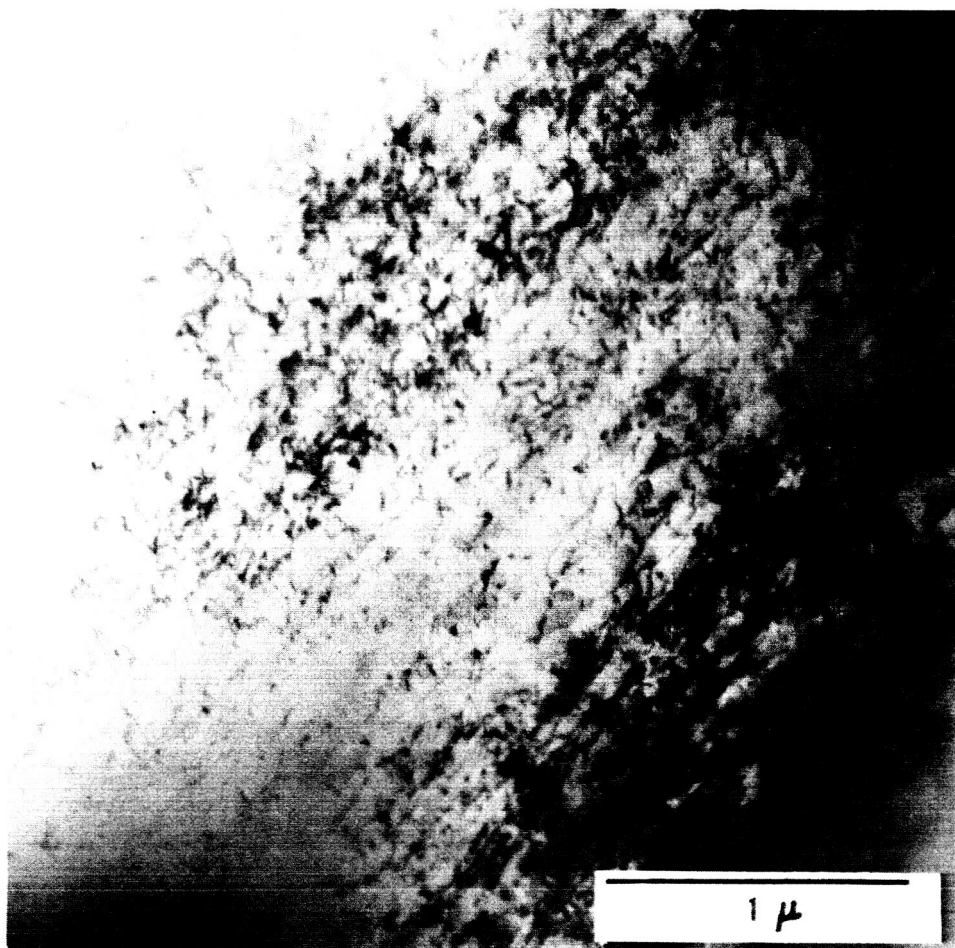
FIGURE 14 - ELECTRON TRANSMISSION MICROGRAPH OF 356-T6

Distance From Chill - 1.06 In.
Strain - 0.57%

1 μ

E13088

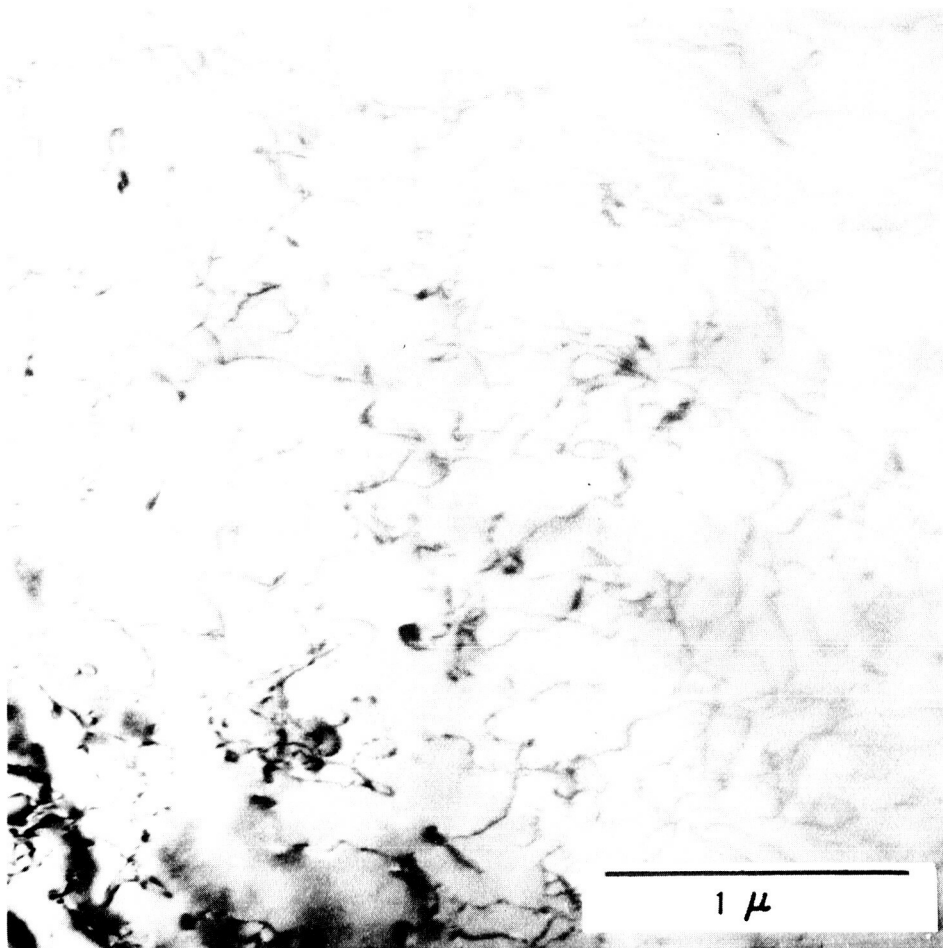FIGURE 15 - ELECTRON TRANSMISSION MICROGRAPH OF 356-T6

Distance From Chill - 2.81 In.
Strain 0.52%

E13114

FIGURE 16 - ELECTRON TRANSMISSION MICROGRAPH OF 356-T6

Distance From Chill - 5.19 In.
Strain - 1% Elongation (Fractured Specimen)
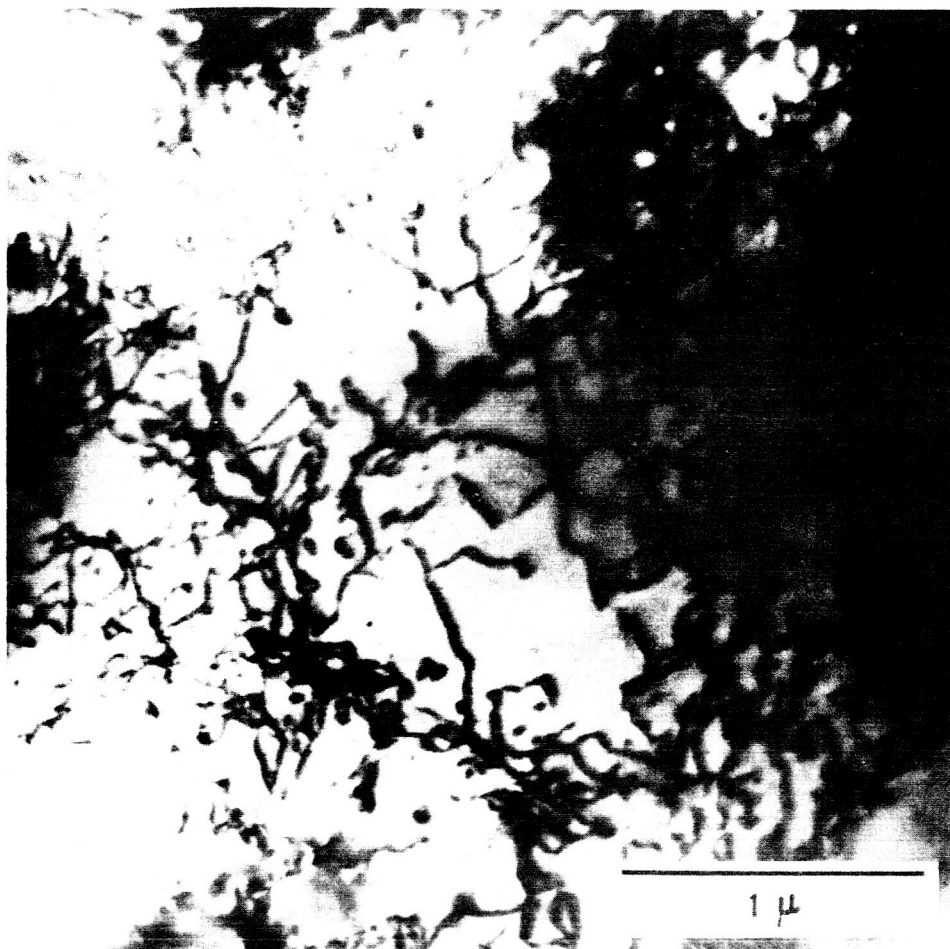0.66% From Load-Strain Record

E13119

FIGURE 17 - ELECTRON TRANSMISSION MICROGRAPH OF 356-T6

Distance From Chill - 6.06 In.
Strain - 0.21%

24

E13122

FIGURE 18 — ELECTRON TRANSMISSION MICROGRAPH OF 356-T6

Distance From Chill — 6.31 In.
Strain — 0.11%

still retain the particles  no differences in dislocation density or distribution were noted in the matrix near the particle.  Figure 13 is an example of this.  The significance of these observations is that each dendrite cell deforms uniformly.

The problem now is to relate the experimental observations to the variations in mechanical properties which result from differences in solidification rate.  Since it has been noted that fracture of the silicon particles is the initial step in gross fracture, consider how such a particle can be stressed.  First, for a specimen loaded in tension, a normal force can be transmitted across the particle-matrix interface. The resulting stress in the particle will be the same as that in the matrix.  For fracture of the particle, both the interface and the matrix must be at least as strong as the particle.  Since the strength of silicon fibers is reported as $5 \times 10^5$ psi, (Reference 7) while ultimate strengths reported here are an order of magnitude lower, it does not seem likely that this mechanism will break many particles.

A way in which appreciable loads can be transmitted to a stronger, non-coherent particle by a weaker, ductile matrix, is by shear stresses across the interface.  This is the same principle used in filament-reinforced materials.  Using the equations developed for composite materials (Reference 8), together with the present data, it can be shown that the length-to-diameter ratio of the particle must exceed 10-15 to develop the fracture stress of the particle.  In these relations, the effective length is in the direction of tensile loading; therefore, this mechanism cannot explain the long fractures normal to the tensile axis noted previously. (Figure 9)

26

Because the silicon particles lie in boundaries between dendrite cells whose orientations may differ, there is another way by which stress may be induced in the particles. For two cells undergoing the same gross strain, there will be a misfit strain at their boundary because of the misorientation of their slip systems. To preserve continuity, this misfit is normally accommodated by an array of dislocations. If an elastic particle is in the boundary, any differential displacement can be accommodated by an elastic strain of the particle. If L is the cell size, $\gamma$ the gross shear strain, and $\theta$ the relative misorientation, then the differential displacement is $L\gamma(1-\cos\theta)$. If D is the silicon particle size, the strain in the particle is the displacement divided by D or $L\gamma(1-\cos\theta)/D$. Since the fracture strain of the silicon particles is approximately a constant ($\sim 2\%$, Reference 7), and the average value of $(1-\cos\theta)$ should not vary appreciably, then for a given particle size, the maximum gross strain for particle fracture should vary as the reciprocal of the cell size. The transition from particle fracture to gross fracture will depend on the matrix properties and the particle size. For a constant matrix strength, an increase in particle size will decrease the number of particle fractures required to decrease the effective load-carrying cross-section to the point of instability and consequent gross fracture. For a constant particle size, an increase in matrix strength will require more broken particles for gross fracture. Here, however, higher strength does not mean higher stress for fracture, but rather, a higher work-hardening rate. While this definition may not be immediately obvious, its validity in connection with the proposed failure model can be demonstrated as follows. Consider a matrix with a very low rate of work-hardening. After yielding, a given amount of strain will cause fracture of some number of particles. The specimen will then be unstable

27

and will fracture because the strength of the matrix cannot increase enough to make up for the loss in cross-sectional area. This conclusion does not depend on the level of stress. Conversely, a high rate of work-hardening will require a greater proportion of fractured particles, which in turn requires additional strain.

To test the proposed model, the elongation data have been plotted as a function of the reciprocal of the average cell diameter in Figure 19. It can be seen that the predicted linear relationship is obtained. There is a minimum elongation of $\sim 1\%$, mainly because the matrix is quite ductile; and, even though enough silicon particles may be fractured at very low strains to cause instability, the local deformation of the matrix as well as misfit of the broken pieces will provide this much deformation. Support for this conclusion is provided by a few tests of 356-T6 on the Instron machine where the plastic strain at ultimate was taken from the load-strain charts. These points, plotted as solid points in Figure 19, form a linear extension of the curve for higher strains.

Increasing the aging temperature of A356-T6, which lowers the work-hardening rate (note the higher yield-ultimate ratio), also lowers the amount of strain required for instability. Since the slope of the curve is $\varepsilon L \cong 2 \delta L = 2 \varepsilon_s D/(1-\cos\theta)$, where $\varepsilon_s$ is the fracture strain of silicon, a change in heat treatment should not alter the slope, which is indeed observed. A decrease in particle size or increase in mis-orientation should lower the slope. Comparing the microstructures of the 356-T6 and the A356-T6 alloys, (Figures 6 and 7) the silicon particle size appears coarser for the 356-T6. On this basis, the slope of the $\delta$ vs 1/L curve should be higher for 356-T6, which is not the case. Apparently
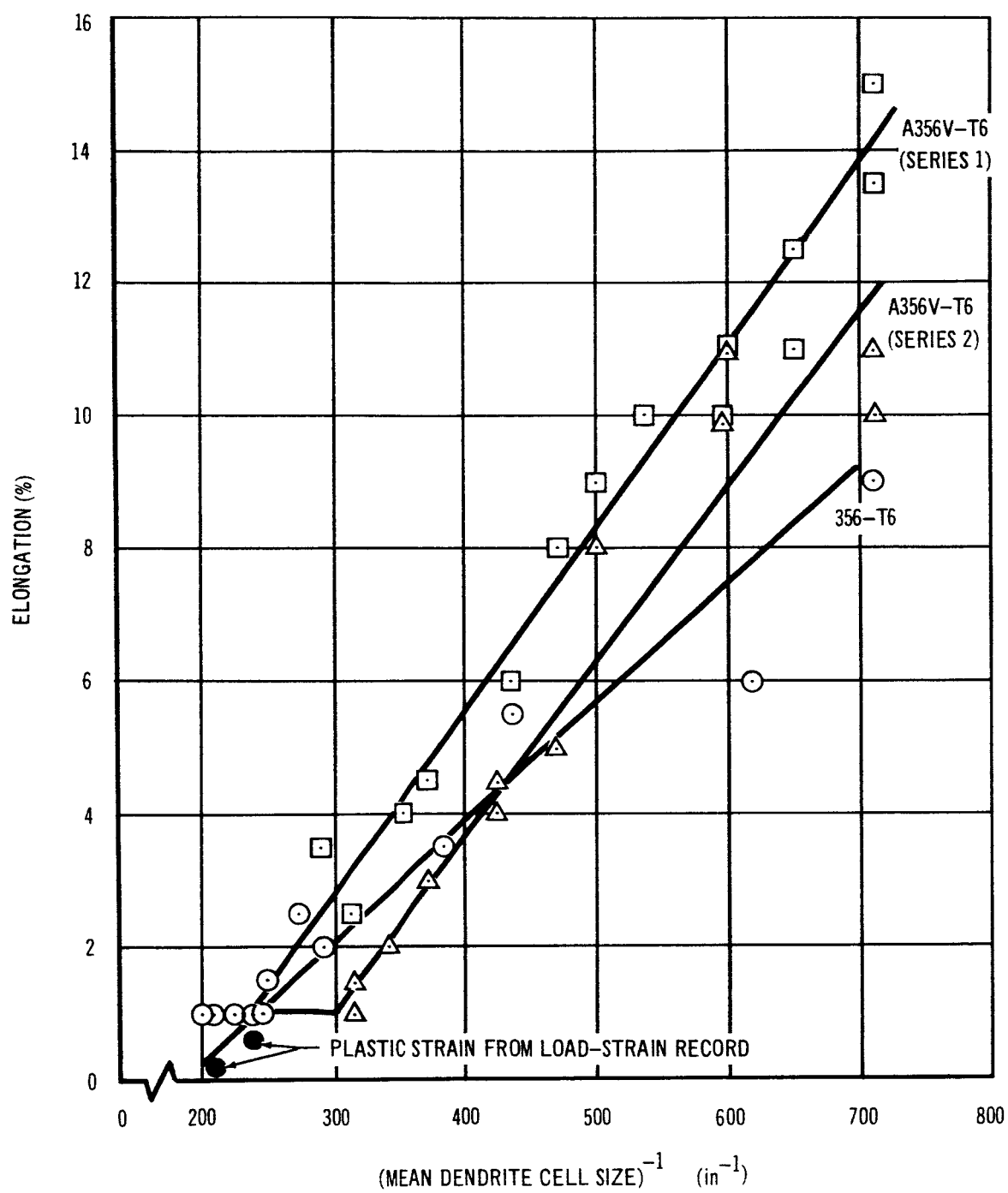
Figure 19.   Elongation vs Reciprocal Dendrite Cell Size

the lower purity of the 356 alloy increases the misorientation.

To estimate the degree of misorientation, take the silicon particle size as $\sim 10^{-4}$ in for A356, L as $10^{-4}$, and $\mathcal{E}_s$ as $\sim .02$. This gives $\theta \approx 11°$ which appears reasonable. The corresponding value for 356 is $\theta \approx 15°$ which is also reasonable.

There are several ways in which the information gained in this study may be applied to improving the properties of weldments and castings. The most obvious is to reduce the dendrite cell size. In this study, cell-size control was by cooling rate. This method cannot always be applied for a variety of reasons, and some other way would be desirable. It is not clear that alloying additions used as grain refiners would perform this function, since cell size and grain size may not be directly related. For example, in this study, practically no difference in grain size was noted for the A356-T6 for the range of solidification times used. This is illustrated by Figure 20. On the other hand, the grain size is certainly the upper limit to the dendrite cell size.

The effect of silicon particle size is not clearly defined. Decreasing the size would decrease the amount of strain required for their fracture, but many more fractures would be required to effect the same decrement of effective cross-sectional areas. A change in distribution of the silicon particles to the interior of the cells would be quite effective since the differential strain of the matrix across the particle would be very small. Decreasing the amount of silicon as particles, either by decreasing the silicon content or increasing the matrix solubility for silicon, should also be helpful.
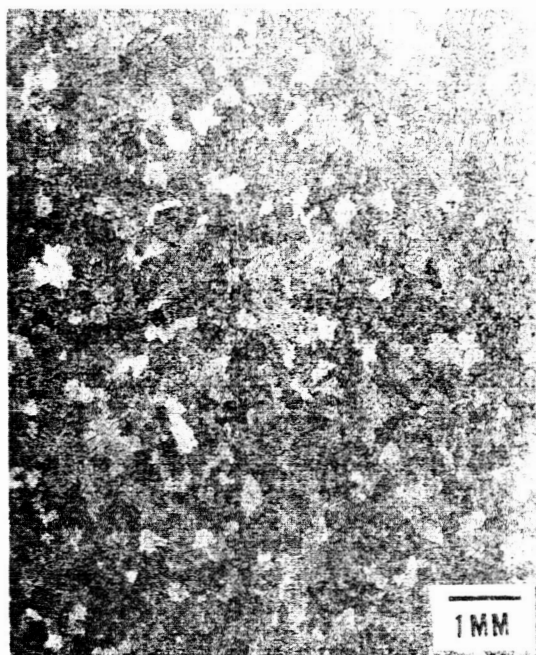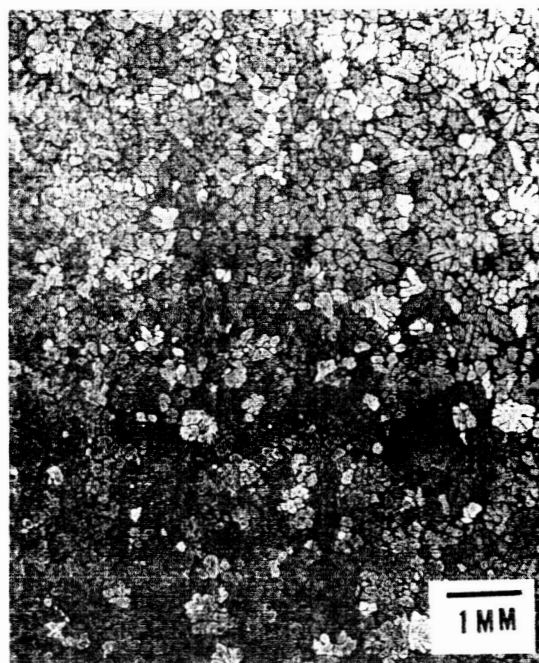
0.5-In. From Chill     MI9766
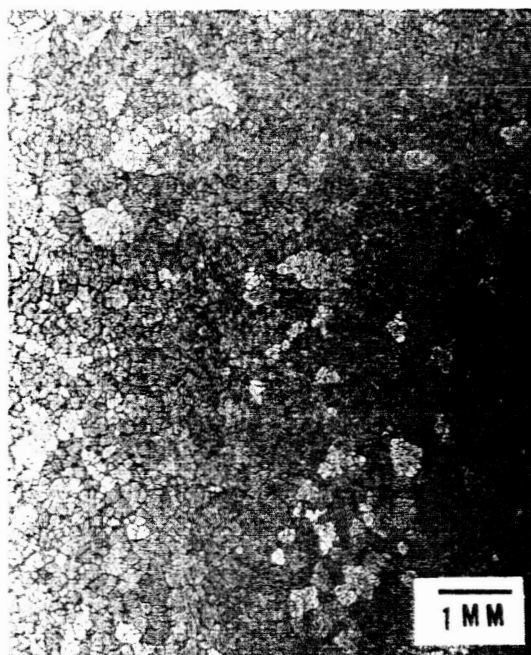
3.5-In. From Chill     MI9768
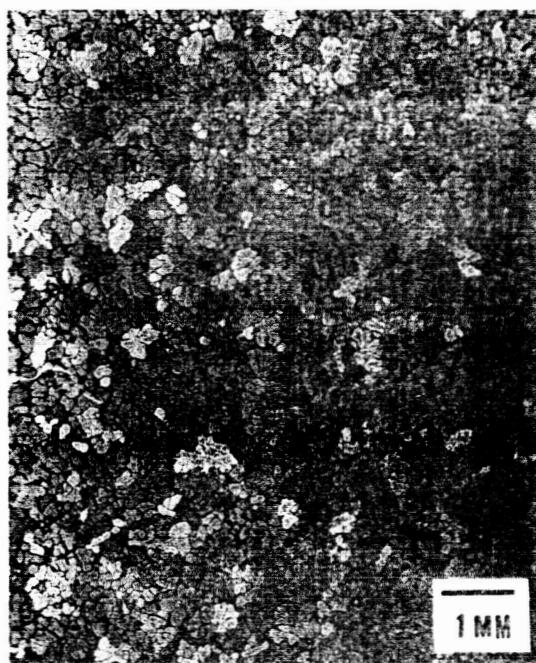
6-In. From Chill     MI9769

8-In. From Chill     MI9770

FIGURE 20 - GRAIN SIZE OF A356-T6

Etchant   10% Copper Sulfate

A decrease in relative misorientation across cell boundaries would improve ductility. The present results suggest that higher Be and Ti may be helpful in this respect, but this has not been proved. Alloying modifications that will increase the work-hardening rate should improve the over-all ductility, provided this does not seriously impair the ductility of the matrix. It is interesting to note, that because of the higher ductility, the fine-celled, low-yield, A356-T6 actually has a higher true stress at fracture than the corresponding material heat treated to a high yield.

4.   CONCLUSIONS

The interrelation of microstructure and fracture mode of 356 type alloys has been studied in detail.

Fracture occurs almost exclusively along dendrite cell boundaries, and initiates in the silicon particles present in those boundaries.

The amount of elongation is inversely proportional to the diameter of the dendrite cells for all sizes smaller than some minimum value.

Yield strength is not a function of dendrite cell size.

Ultimate strength is controlled by the dendrite cell limitation on elongation.

The maximum cell size for enhanced elongation is a function of the work-hardening rate of the matrix.

5. <u>REFERENCES</u>

1. H. J. Rowe, <u>Metals Handbook,</u> American Society for Metals, Cleveland, 1948, p 763.

2. W. A. Bailey, "The Effect of Solidification Rate Upon the Fatigue Behavior of Cast A356 Variant -T6 Type Aluminum Alloy", Douglas Paper No. 3005A, May, 1965.

3. W. A. Bailey "The Effect of Solidification Rate Upon the Fatigue Behavior of Cast A356 Variant-T6 Type Aluminum Alloy, Part II, Influence of Ductility" Douglas Paper No. 3005B,

4. E. M. Passmore, M. C. Flemmings, & H. F. Taylor "Fundamental Studies on the Effects of Solution Treatment, Iron Content, and Chilling of Sand Cast Aluminum-Copper Alloy", Modern Castings, March, 1958.

5. A. Phillips, V. Kerlins, & B. V.Whiteson, "Electron Fractography Handbook", ML-TDR-64-416, Jan. 31, 1965.

6. T. A. Despres, "Application of a Conducting Mask for Thinning Metallic Foils for Electron Transmission Microscopy", the University of Michigan, Department of Mechanical Engineering (cir. 1963).

7. W. C. Dash, Growth and Perfection of Crystals, J. Wiley, New York, 1958.

8. A. Kelly and G. J. Davies, "The Principles of the Fiber Reinforcement of Metals", Met. Reviews, 10, 1 (1965).

S.O. 5760-1101

EWO 28495

S.A. 7115, Tech. Record No. 04444